nature nanotechnology

SUPPLEMENTARY INFORMATION

DOI: 10.1038/NNANO.2011.211

A surface-anchored molecular four-level conductance switch based on single proton transfer

Willi Auwärter, Knud Seufert*, Felix Bischoff, David Ecija, Saranyan Vijayaraghavan, Sushobhan Joshi, Florian Klappenberger, Niveditha Samudrala, and Johannes V. Barth*

1. Molecular conformation of 2H-TPP/Ag(111)

To clarify the conformation of the 2H-TPP molecules anchored on a Ag(111) surface, we combine scanning tunneling microscopy (STM) with complementary near-edge x-ray absorption fine structure (NEXAFS) experiments. This approach prooved to be very powerful to resolve the conformation of surface anchored porpyrins[1-3], as the NEXAFS technique is sensitive to the orientation of molecular orbitals with respect to the substrate while STM yields local information. The STM images (Fig. 1 and Fig. S1e) exhibit a two-fold symmetric appearance of 2H-TPP/Ag(111). The quantitative analysis of the NEXAFS data shows that this effect originates in terminal groups rotated out of the surface plane together with a moderate saddle-shape deformation of the porphyrin macrocycle.

Figure S1 a shows angular dependent NEXAFS spectra of the carbon K-edge of a submonolayer coverage of 2H-TPP/Ag(111), dominated by four peaks in the π region (284.3 eV, 285.3 eV, 287.3 eV und 289.0 eV) and a broad δ structure. For the analysis, we focus on the leading edge of the π range, where a separation of the spectral features of different molecular groups is evident. Following earlier reports, we fit the C1s NEXAFS spectra by two sets of features representing the phenyl groups (blue curves in Fig. S1c) and the macrocycle (green curves in Fig. S1c), respectively. For a detailed discussion please refer to Ref.[3].

DOI: 10.1038/NNANO.2011.211

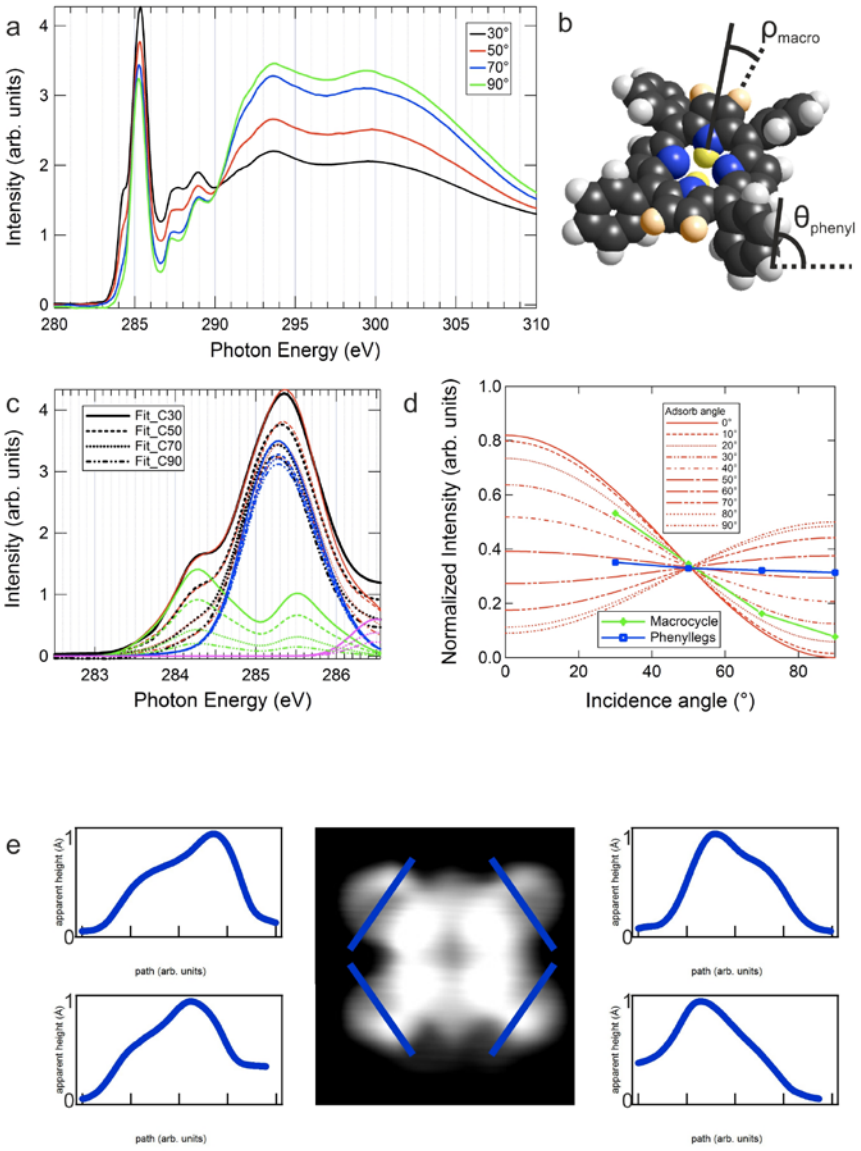

Fig. S1: Adsorption induced deformation of 2H-TPP (a) Carbon K edge NEXAFS spectra of about one monolayer of 2H-TPP on Ag(111). The different colors represent different angles between the electric field vector of the x-ray beam and the surface normal. (b) Structural model highlighting the adsorption induced saddle-shape deformation of 2H-TPP on Ag(111) and the corresponding angles discussed in d. (c) Deconvolution of the leading edge into spectral parts originating from the macrocycle (green) and the phenyl substituents (blue). (d) The angular dependence of the two moieties: ρ_{macro} = 25° (green) and θ_{phenyl} = 53° (blue). (e) STM image resolving the phenyl substituents. The height profiles taken along the blue lines are asymmetric and visualize the rotation of the phenyl groups by the angle θ_{phenyl}.

The angular dependence of the intensities of the phenyl and macrocyle related features extracted from the fitting procedure is shown in Figure S1 c together with calculated curves. The comparison yields an average angle of 53° degrees between the phenyl rings and the surface plane and an average angle of 25° between the pyrrole rings in the macrocycle and the surface plane. Combining the

symmetry observed in the high-resolution STM data (see Fig. 1) with these angles extracted from the NEXAFS analysis, we conclude that 2H-TPP/Ag(111) shows a slight saddle-shape deformation where one pair of opposite pyrrol rings is tilted upwards by approximately 25° (α-pyr) (see model in Fig. S1 b orange hydrogens), while the other pair is bent downwards by the same angle (κ-pyr). In addition the phenyl groups are alternately rotated out of the surface plane exhibiting a dihedral angle of approximately 53°. Consequently, height profiles across the phenyl substituents extracted from STM images appear asymmetric (see Fig. S1e). The resulting inequivalence of the two pairs of pyrrole rings also influences the switching probability (compare section 2).

2. Visualization of the spatial dependence of the switching probability

To determine the local switching probability of 1H-TPP/Ag(111) dI/dV maps were recorded together with constant current STM images at – 2V sample bias and 0.5 nA tunneling current. At these values the switching rate is above 1 per second (cf. Fig. 5). The scan speed was set to 0.38 lines per second to cover several switching events. Indeed, the topographic images (Fig. S2, grayscale) show a noisy appearance due to the movement of the inner hydrogen. The dI/dV signal, superimposed in red and blue, visualizes single switching events, as a switch means a steplike change in the conductance, resulting in a sharp spike (blue) or dip (red) in the dI/dV signal. Fig S2 reveals an enhanced switching probability above two of the four pyrrole rings. This pair corresponds to the two α-pyr moieties. The switching rate on the κ-pyr and on the terminal groups is clearly lower. To rule out an effect of the fast scan direction on the spatial dependence of the switching probability, the scan direction was rotated by 90° in Fig. S2 b. Consistently, the highest switching probability is observed above the two α-pyr rings. These data are in complete agreement with Figure 1 g in the manuscript visualizing the spatial dependence of the switching rate for 2H-TPP.

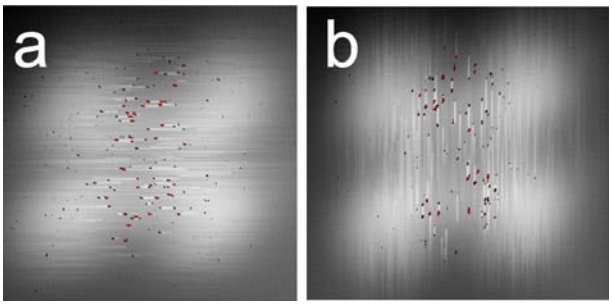

DOI: 10.1038/NNANO.2011.211

Fig. S2: Real-space resolved local switching by a superposition of topographic STM images (grayscale) with dI/dV maps (red and blue) (I=0.5 nA, U=-2V, scan speed to 0.38 lines/s). a, Fast scan direction horizontal. b, Fast scan direction vertical (rotated by 90°). Compare Fig. 1 for the spatial dependence of the switching rate in the 2H-TPP case.

3. Double proton transfer in two-dimensional arrays

An ideal molecular switch should be integrable into well-defined nanoscale architectures. As the molecular switch presented here bases on proton transfer in the inner pocket of the porphyrin, the peripheral groups controlling the aggregation of porphyrin modules into regular assemblies are not affected by the operation of the switch. Fig. S3 presents an example of a highly ordered square array of 2H-TPP/Ag(111). Indeed, the switching performance is sustained in this regular pattern as exemplified by the image sequence in Fig. S3. This example highlights not only the self-assembly of arrays of molecular switches, but suggests the use of such systems as molecular memories: The position of the hydrogen might be used to encode and store information. However, we should point out that the switching in 2H-TPP arrays shows non-local effects, in contrast to the switching on individual 2H-TPP that was local. In particular, we observed proton transfer in molecules up to 4 nm away from the module where the tip was positioned during the current pulses.

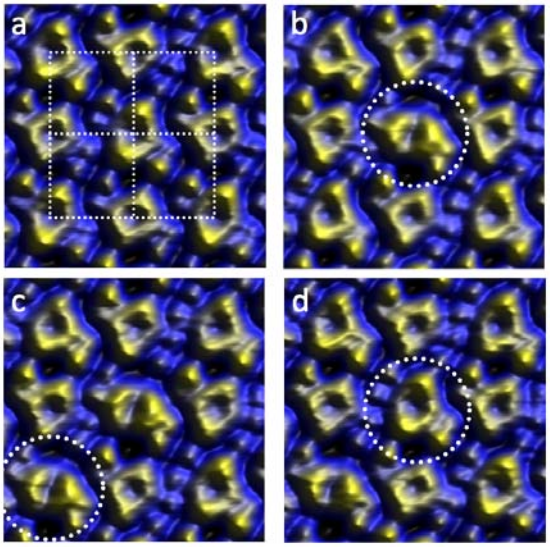

Fig. S3: Highly ordered array of 2H-TPP/Ag(111). a, STM image of nine 2H-TPP molecules in configuration H_{α} positioned on a square lattice highlighted by the dashed lines. b-d Switching of individual modules in the array between configuration H_{α} and $H_{\alpha'}$. The 2H-TPP molecules that were transformed are labeled by dashed circles in the given image frame. The proton transfer is completely reversible: The array of molecular switches can be reset by returning to the situation represented in a (*I*=0.1 nA, *U*=-0.2 V).

4. Statistical analysis of the distribution of switching times

In addition to the analysis of the switching rates as a function of current (see Fig. 4), the distribution of the switching times was explored as a function of the tunneling current I. To this end, the residence times in a given current level were evaluated and displayed in histograms (see Fig. S4 a-d). These data follow Poisson statistics and are fitted by an exponential function, where the decay constant R corresponds to the switching rate. Fig. S4 e shows a plot of these rates as a function of tunneling current I. As revealed by the fit, the rates follow a power-law, where the rate is proportional to I^N with N = 1.08 ± 0.1. This finding confirms that the switching bases on independent one-electron processes.

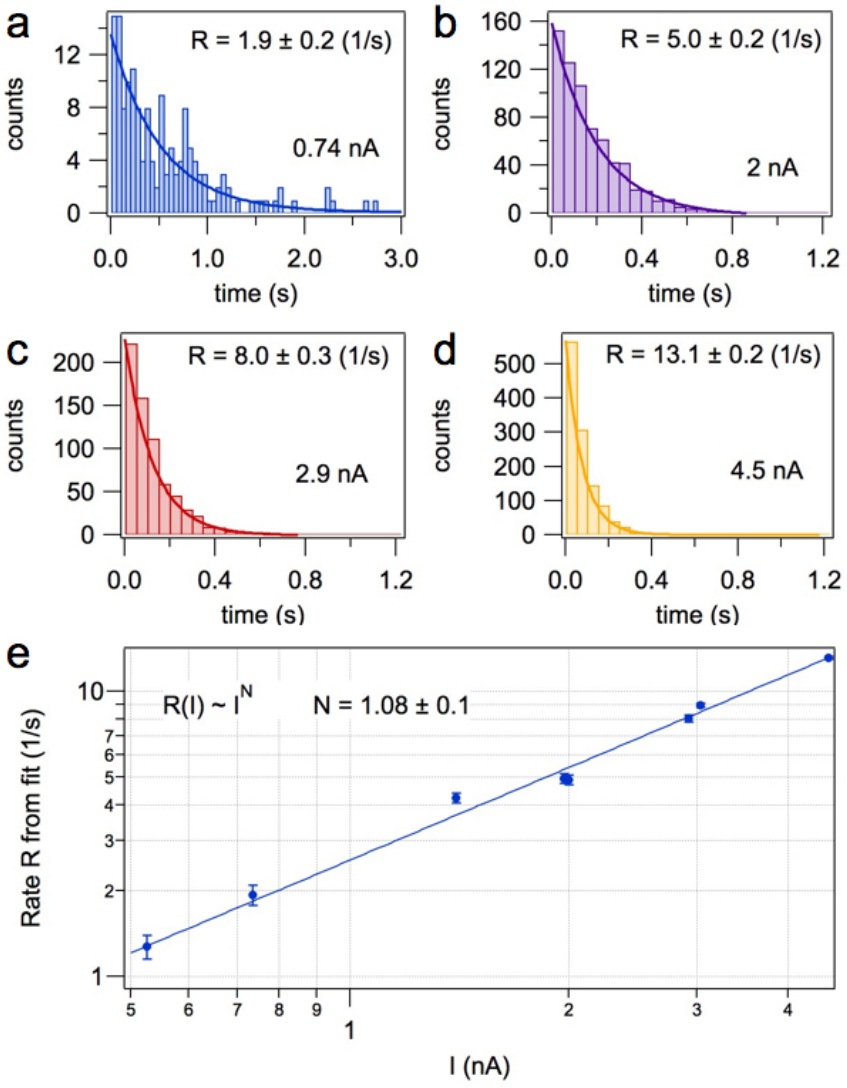

Fig. S4: Analysis of the switching times for 2H-TPP. a-d, Exponential distribution of the switching times for different currents I at -1.6 V. Note the different time scale in a and b-d, respectively. e, Switching rates extracted from the exponential fits as a function of tunneling current. The solid line represents a power-law fit to the data, yielding N = 1.08 ± 0.1 and thus confirming independent one-electron processes triggering the switching.

DOI: 10.1038/NNANO.2011.211

5. Comparison of I(t) spectra on α-pyr and κ-pyr moieties in 1H-TPP

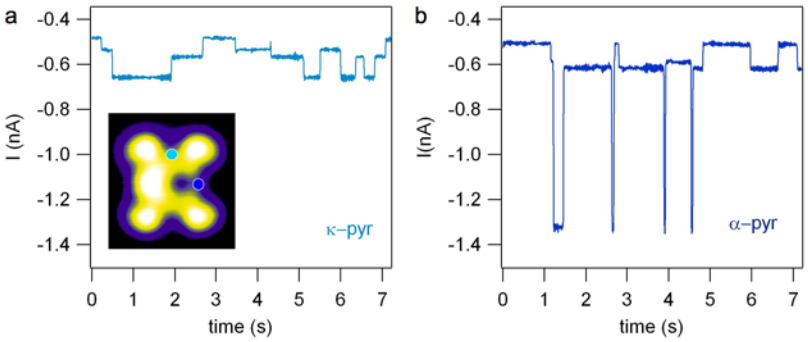

Fig. S5: Comparison of I(t) switching curves recorded with the very same tip on the very same 1H-TPP on α-pyr and κ-pyr positions, respectively. a, On the κ-pyr position, the four current levels are closely spaced but clearly resolved, as shown in Fig. 3 in the article. The inset highlights the position on 1H-TPP where the spectra reproduced in a and b were recorded. b, on the α-pyr position, again four current levels can be discriminated. However, the current level spacing in the I(t) spectra is strikingly different: In case the hydrogen is located on the α-pyr position where the tip is positioned, the current level is about a factor 2.6 higher than for the opposite α-pyr position. Both spectra were recorded after stabilizing the tip at *I*=0.5 nA and *U*=-1.6 V.

6. Influence of tip termination on switching rate

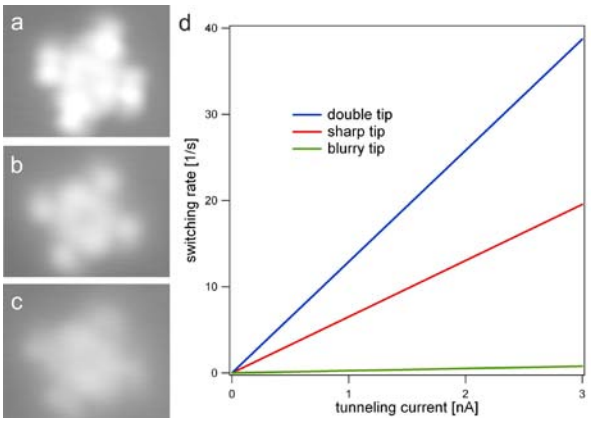

Fig. S6: Effect of the tip termination on imaging and switching. Figs. a-c show topographic STM images of 2H-TPP recorded with drastically different STM tip terminations. a represents a double-tip, b a regular tip with good resolution as regularly used in the experiments and c a very blurry tip. The influence of of the tip termination on the switching rate is outlined in d comparing linear fits of the rates for the three tips. The switching rates varies strongly, with higher rates for sharper tips (*I*=0.5 nA and *U*=-1.6 V).

7. Analysis of 1H-TPP switching rates

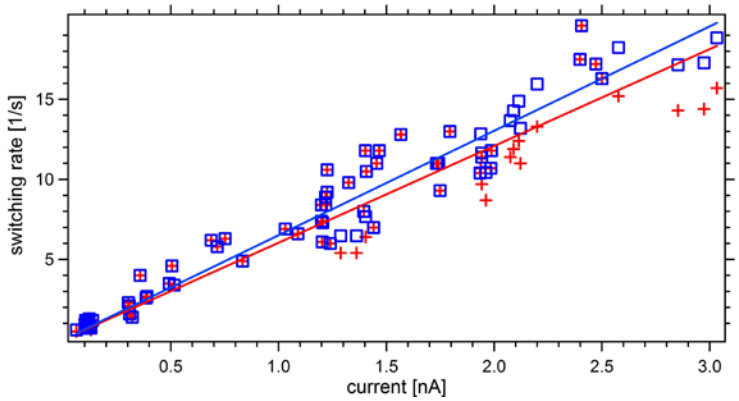

Fig. S7: Corrected (red crosses) and the originally counted values (blue squares) and the corresponding fitted lines, which are forced to go through zero counts in the absence of a tunneling current. Applying this correction generally yields a slightly increased switching rate (in this example *S* amounts to 6.52 ± 0.11 $s^{-1}nA^{-1}$ compared to the raw data where *S* equals 6.05 ± 0.14 $s^{-1}nA^{-1}$), while the quality of the linear fit is improved.

For the 1H-TPP case it is, depending on the precise position and symmetry of the tip, possible, that two of the four conductance levels are indistinguishable. Therefore we used a correction factor of 6/5 for all counted switches in the I(t) spectra exhibiting only three discriminable levels. 6/5 is used because two of all 12 possible transitions can not be resolved. For high switching rates it becomes harder to discriminate between neighboring levels, due to the shorter lifetime in a single current level in the I(t) spectrum.

8. Tunability of the switching rate

Fig. 4 and 5 in the article reveal that both higher currents and higher sample bias voltages lead to an enhanced switching rate. However, the applicable voltage is limited by the deprotonation threshold, and currents above 5 nA (at a sample bias of -2V) can induce a lateral displacement of the 2H-TPP molecules. By approaching *U* and *I* to these intrinsic limits, switching rates of up to 600 Hz can be achieved (cf. Fig. S8).

DOI: 10.1038/NNANO.2011.211

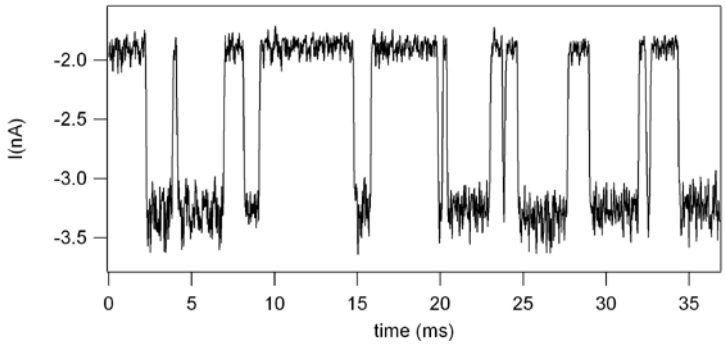

Fig. S8: Fast switching of 2H-TPP/Ag(111). Current versus time trace recorded at -2 V exhibiting 21 switches between two current levels within 35 ms, corresponding to a rate of approximately 600 Hz.

9. References

1. Auwärter, W. et al. Conformational Adaptation and Selective Adatom Capturing of Tetrapyridyl-porphyrin Molecules on a Copper (111) Surface. J. Am. Chem. Soc. 129, 11279-11285 (2007).
2. Weber-Bargioni, A. et al. Visualizing the Frontier Orbitals of a Conformationally Adapted Metalloporphyrin. ChemPhysChem 9, 89 (2008).
3. Auwärter, W. et al. Site-specific electronic and geometric interface structure of Co-tetraphenyl-porphyrin layers on Ag(111) Phys. Rev. B 81, 245403 (2010).